International Journal of Medical Physics, Clinical Engineering and Radiation Oncology, 2025, 14(3), 89-99
https://www.scirp.org/journal/ijmpcero
ISSN Online: 2168-5444
ISSN Print: 2168-5436

Performance Evaluation of Ionization Chambers and Microdiamond Detectors in Small Field Penumbra Measurements

Ntombela N. Lethukuthula[1,2], Mohlafase Lerato[2], Rovetto J. Nicolas[1], Shivambu I. Gezani[1,2]

[1]Department of Radiation Oncology, Steve Biko Academic Hospital, Pretoria, South Africa
[2]Department of Medical Physics, University of Pretoria, Pretoria, South Africa
Email: lethukuthula.ntombela@up.ac.za

How to cite this paper: Lethukuthula, N.N., Lerato, M., Nicolas, R.J. and Gezani, S.I. (2025) Performance Evaluation of Ionization Chambers and Microdiamond Detectors in Small Field Penumbra Measurements. *International Journal of Medical Physics, Clinical Engineering and Radiation Oncology*, **14**, 89-99.
https://doi.org/10.4236/ijmpcero.2025.143007

Received: May 14, 2025
Accepted: June 30, 2025
Published: July 3, 2025

Abstract

In small-field radiotherapy, accurate characterization of the penumbra is critical for precise dose delivery, particularly in treatments like stereotactic radiosurgery (SRS), where steep dose gradients are required to spare surrounding healthy tissues. The objective of this study was to quantify the penumbra region in small radiation fields to improve dose delivery accuracy and minimize unnecessary exposure. Three detectors—the Semiflex 3D ion chamber, PinPoint 3D ion chamber, and microDiamond detector—were used to measure beam profiles for field sizes ranging from 1 × 1 cm^2 to 4 × 4 cm^2 using 6 MV photon energy. These measured profiles were compared against data from the Monaco treatment planning system (TPS) to evaluate consistency and detector performance. For larger field sizes (4 × 4 cm^2 and 3 × 3 cm^2), the Semiflex 3D detector showed the smallest deviations from TPS data, with errors of 14.5% and 14.3%, respectively. The PinPoint 3D and microDiamond detectors exhibited larger deviations, with microDiamond showing the greatest discrepancies (30.7% and 34.5%). In the 2 × 2 cm^2 field, Semiflex maintained a deviation of 14.9%, while PinPoint 3D and microDiamond showed errors of 28.1% and 38.4%. For the smallest field (1 × 1 cm^2), all detectors underestimated penumbra width: 11.3% (Semiflex 3D), 27.1% (PinPoint 3D), and 32.7% (microDiamond). Despite strong overall correlations between measured and planned profiles, noticeable deviations were observed, particularly in smaller fields. The Semiflex 3D, with the largest collecting volume, showed the best agreement with TPS data across all field sizes. This study highlights the importance of detector selection in small-field dosimetry and underscores the need for accurate penumbra quantification to ensure optimal treatment outcomes.

Keywords

Detectors, Small-Field, Beam-Profile, Penumbra

1. Introduction

In radiation therapy, accurate beam delivery is crucial for maximizing tumor control while minimizing damage to surrounding healthy tissues [1]. A key factor in achieving this precision is understanding the characteristics of the radiation beam, which can be influenced by the detectors used to measure beam data. In small-field radiotherapy, various treatment techniques are designed to precisely target localized, small tumors or lesions with high-dose radiation. These techniques include intensity-modulated radiotherapy (IMRT), volumetric modulated arc therapy (VMAT), and stereotactic radiosurgery (SRS) [2].

Stereotactic radiosurgery (SRS) is a precise radiotherapy technique for treating small, well-defined brain lesions using multiple focused high-dose radiation beams, minimizing exposure to nearby healthy tissue [3] [4]. Key features include small target volumes, few treatment sessions, and high doses per fraction [5]. Field sizes are typically under 4 cm, with critical structures often nearby, requiring high spatial (±1 mm) and dose (±5%) accuracy and steep dose gradients to protect normal tissue [6]. Sharp beam edges enable smaller margins, though steep dose falloff remains a limiting factor in sparing adjacent critical structures [7]-[9]. The radiological penumbra is primarily caused by the scattering of photons and the generation of secondary electrons within tissue. Its extent increases with higher beam energies and decreases in tissue density. In small fields (less than 4×4 cm^2), the penumbra is mainly influenced by the range of secondary electrons [10]-[12].

In this study, small-field beam profiles measured using various detectors are compared with Monte Carlo-generated profiles from the Monaco treatment planning system to evaluate the accuracy and reliability of both measurement techniques and computational models. The primary aim is to quantify the penumbra region in small-field radiotherapy, thereby enhancing dose delivery precision and minimizing exposure to surrounding healthy tissues. Given the relatively broad penumbra in small fields, accurate measurement is crucial for ensuring adequate target coverage while preventing overdose to nearby organs. This approach also contributes to improving the accuracy of treatment planning systems by addressing challenges such as electron disequilibrium and detector limitations. Additionally, it supports quality assurance through profile comparisons and may impact biological outcomes by influencing tumor control, complication probabilities, and margin design.

2. Materials and Methodology

2.1. Data Collection

Both raw data and TPS data were collected. Each of these processes has been out-

lined. The materials that were used to collect the raw data included the three detectors, which have been summarised in Table 1, as well as a PTW Beamscan water phantom, together with the PTW Trufix positioning tools. The linear accelerator that was used was an Elekta Versa HD. The TPS data was generated using the Monaco TPS, using the same set-up parameters that were used when the raw data was collected, and the python software was used for data analyses.

The detectors that were used had been calibrated within the recommended calibration frequency, at a recognised secondary standard dosimetry laboratory (SSDL). Each of them had a calibration certificate to indicate this.

2.1.1. Measurements with detectors

The three detectors that were used to collect the raw data are summarised in Table 1.

Table 1. Detectors used to collect raw data [13] [14].

DETECTOR	TYPE	SENSITIVE VOLUME	SENSITIVE RADIUS
PTW Semiflex 3D [6]	Ionization chamber	0.07 cm^3	2.40 mm
PTW PinPoint 3D [7]	Ionization chamber	0.016 cm^3	1.45 mm
PTW microDiamond [8]	Solid state detector	0.004 mm^3 (0.000004 cm^3)	1.10 mm

Data was collected with each of the detectors using the same Elekta Versa HD linear accelerator and the same set-up parameters. The PTW Beamscan water tank phantom was used as the phantom material and for positioning each of the detectors, accompanied with the PTW Trufix detector positioning tools. The PTW BeamScan tank which was used has an 'Auto Beam-Alignment' function, which automatically finds the central position of the beam, and adjusts the detector's position so that it is at the beam's centre. This functionality was used before using each of the detectors. This was validated with the first few profiles that were taken with each detector, ensuring that the profiles were accurately centred on the set of axes. The set-up parameters that were used are summarised in Table 2.

Table 2. Set-up parameters that were used to collect the raw data.

SETUP PARAMETERS	
Source to Surface Distance (SSD)	100 cm
Photon Energy	6 MV
Field Size	1 × 1 cm^2, 2 × 2 cm^2, 3 × 3 cm^2, 4 × 4 cm^2
Measurement Depth (for beam-profiles)	10 cm

The data were collected for each of the detectors, for each field-size and depth (for the beam-profiles). Continuous scans were measured, using the smallest res-

olution for each detector. Each measurement was repeated three times, and an average between the three was obtained, which is what was used for the research. There were no large or noticeable discrepancies between the repeated measurements.

2.1.2. Monaco Treatment Planning Data

To generate the Monte Carlo data on the TPS, the experimental setup used during data collection was replicated. The dose distribution was then calculated, and the dose data was extracted, as described below.

A uniform phantom ($30 \times 30 \times 30$ cm^3 cube) was imported into Monaco, contoured, and assigned a uniform electron density equivalent to water. A single anteroposterior (AP) beam was created, prescribing 1.0 Gy to the center of the phantom at a depth of d_max (1.5 cm). The setup used a source-to-surface distance (SSD) of 100 cm and an initial field size of 4×4 cm^2. The Monte Carlo dose calculation algorithm was employed, using a calculation matrix of 0.1 mm and an error threshold of 0.5%.

Following dose calculation, coronal dose planes were exported at a depth of 10 cm—matching the depth at which the raw data was measured. Additionally, a transverse dose plane passing through the center of the phantom was exported.

The exported dose planes were analyzed using VeriSoft software, which was used to extract beam profiles from the coronal dose planes and percentage-depth-dose (PDD) data from the transverse dose plane. This process was repeated for all field sizes used during data collection, including 3×3 cm^2, 2×2 cm^2, and 1×1 cm^2.

2.2. Isodose Lines Generation (Decrement Line Method)

Figure 1. Decrement lines converging from a point source (adapted from Hidaytalla [15]).

As an additional means of comparing the detectors to each other and to the TPS data, the isodose distributions generated by the different sets of data were investigated. The 'decrement lines' process, as described in a thesis submitted by Hiday-

talla [15], was used for this analysis. The process of generating the isodose distributions is described in this section. The decrement lines method was chosen for this research because there has not been much work done using the decrement line method, so it served as a niche tool to use to evaluate the differences between the detectors. This became especially useful when considering the number of papers produced using more common methods such as the gamma index analysis or dose difference maps.

The decrement line method is based on the assumption that decrement lines exist, which connect points of equal dose values. An assumption is made that if the decrement lines are extended, they converge to meet at a point source, as indicated in **Figure 1**. The decrement line method is then performed as follows:

If X_0 is the dose value that we are interested in (*i.e.*, this is the isodose value that we want to determine), then the value, X_{iso}, that is equal to X_0 on a given decrement line, D_i, corresponds to a (dose) value in the central axis at the same depth given by:

$$X = X_{\text{iso}} \times \frac{100}{D_i} \tag{1}$$

Equation (1) allows for determining the values, X, along the central axis that are equivalent to any given isodose, X_{iso} due to a given decrement line, D_i. Using these dose values, together with the PDD values for the specific field size and energy that we are concerned with, we are able to determine the depth of that dose value in the phantom, which is the same depth as the value of the given isodose line, along the central axis, due to a given decrement line. The trigonometric relation between the depth (the sum of the SSD and depth in the phantom), the width (the distance along the x-axis), and the take-off angle, α, is thus given by:

$$\tan(\alpha) = \frac{x}{\text{SSD} + y} \tag{2}$$

The next assumption that is made for the decrement process (which has been justified by Hidaytalla [15]) is that the take-off angles are nearly constant for all relevant depths. This is useful, as the next step in the process is to determine the widths (x-values) which correspond to the depths (y-values) determined using Equation (2). Since we know that the take-off angle is constant for different depths, if we know the take-off angles for a given depth and field size, we can use the same angles for other depths at the same field size. Thus, using the beam-profile data, the take-off angles can be directly determined.

After determining the take-off angles (α) and depths (y), we can directly determine the widths (x) for any isodose line, due to a given decrement line. By collecting the required data, which only includes a single beam profile and PDD for its most basic form, the isodose distributions can be generated for any depth, due to each decrement line.

The decrement line process as described above was coded, and the results plotted, using the Python programming language, to get a visual representation of the

isodose distributions. A quantitative analysis was also performed based on the results obtained during this process. This method was used to analyse and compare each of the two sets of data (raw and TPS generated).

3. Results

The initial results include the measured beam-profile data, which is compared to the TPS data obtained through Monte Carlo calculations performed on the Monaco TPS. The raw profiles that were measured, together with the TPS-generated data profiles, have been plotted in Figure 2 for each of the four field sizes.

Table 3 presents a comparative analysis of penumbra measurements between TPS data and raw data obtained from three different detectors—Semiflex 3D, PinPoint 3D, and MicroDiamond—across various field sizes (4×4 cm^2 to 1×1 cm^2). The TPS data serves as a reference for ideal or benchmark penumbra values, against which the deviations of raw data from each detector are evaluated. As the field size decreases, the discrepancy between the TPS data and the detector measurements generally increases, with the MicroDiamond detector showing the largest percentage deviations, especially for smaller field sizes. These variations highlight the impact of detector characteristics on dose profile accuracy in small field dosimetry.

Table 3. Penumbra results for golden data versus raw data.

FIELD SIZE (cm^2)	TPS DATA PENUMBRA (mm)	SEMIFLEX 3D		PINPOINT 3D		MICRODIAMOND	
		PENUMBRA (mm)	DEV.	PENUMBRA (mm)	DEV.	PENUMBRA (mm)	DEV.
4×4	6.606	5.616	14.5%	4.757	28.0%	4.581	30.7%
3×3	6.306	5.405	14.3%	4.625	26.7%	4.129	34.5%
2×2	6.006	5.109	14.9%	4.316	28.1%	3.670	38.4%
1×1	5.105	4.529	11.3%	3.722	27.1%	3.435	32.7%

4. Discussion

4.1. Penumbra

The comparison of penumbra widths on Table 3. between the Monte Carlo-generated data and the measured raw data from different detectors reveals notable discrepancies. These deviations highlight the impact of detector choice on accurately characterizing beam edges, particularly in small-field dosimetry.

For all field sizes, the measured penumbra values were consistently lower than the TPS data, indicating that the detectors may underestimate the true penumbra width. This discrepancy is likely influenced by detector-specific factors, including spatial resolution, volume averaging effects, and intrinsic response characteristics.

At larger field sizes (4×4 cm^2 and 3×3 cm^2), the Semiflex 3D detector demonstrated the smallest deviation from the TPS data, with errors of 14.5% and 14.3%, respectively. In contrast, the PinPoint 3D and MicroDiamond detectors showed significantly larger deviations, with the MicroDiamond detector exhibiting the

highest discrepancies (30.7% for 4 × 4 cm^2 and 34.5% for 3 × 3 cm^2). The sharper fall-off in measured penumbra for these detectors suggests a higher spatial resolution but also indicates potential underestimation due to their smaller sensitive volume.

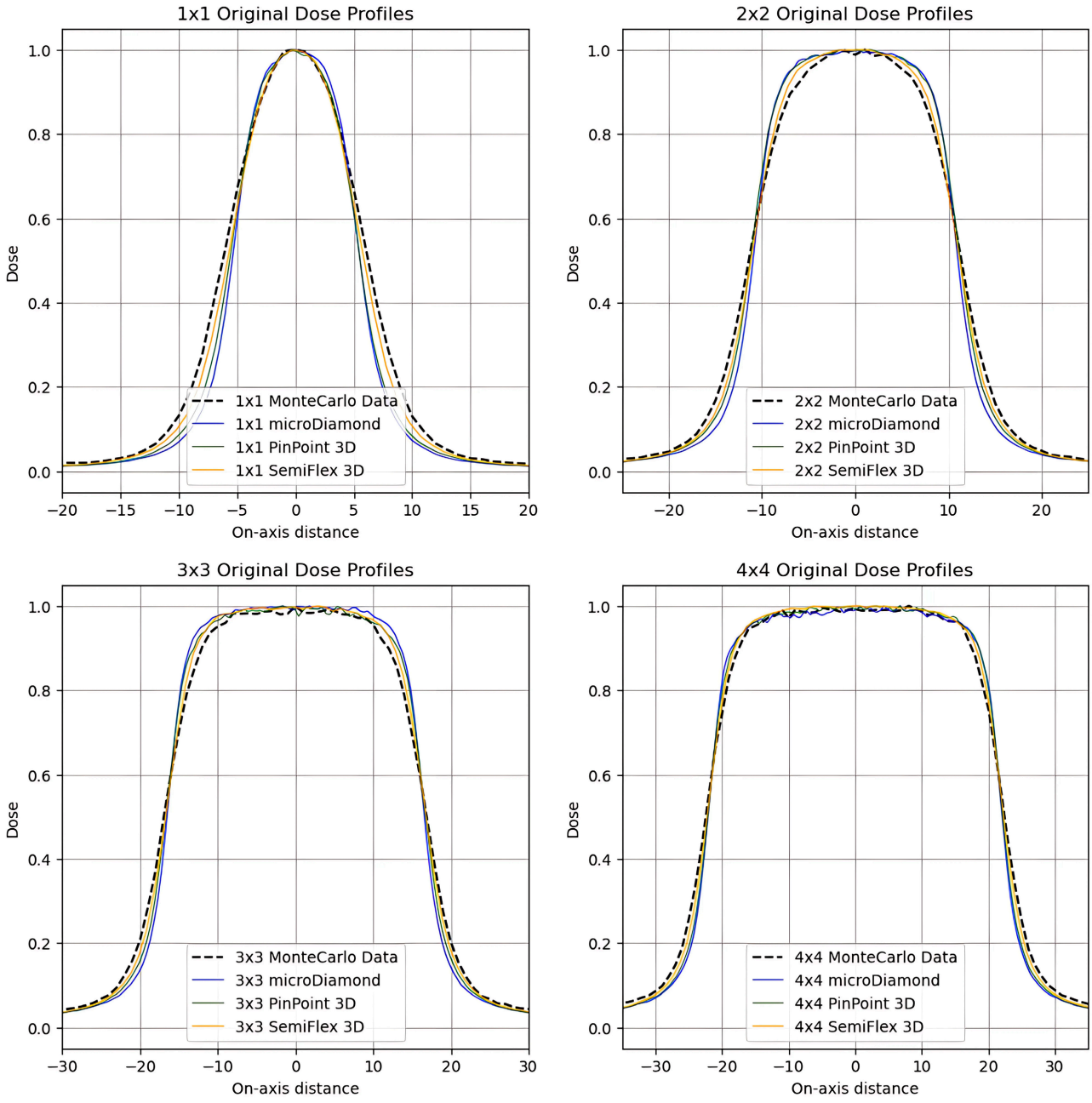

Figure 2. Monte Carlo TPS data profiles versus raw data measured for each chamber.

As the field size decreased, deviations became more pronounced. For the 2 × 2 cm^2 field, the Semiflex 3D detector maintained a deviation of 14.9%, while the PinPoint 3D and MicroDiamond detectors showed errors of 28.1% and 38.4%, respectively. The increasing deviation with decreasing field size suggests that

smaller detectors may struggle with accurate penumbra characterization due to their response to lateral dose gradients.

For the smallest field size (1×1 cm^2), all detectors continued to underestimate the penumbra width, with deviations of 11.3% (Semiflex 3D), 27.1% (PinPoint 3D), and 32.7% (MicroDiamond). Although the Semiflex 3D detector exhibited the lowest deviation, its relatively larger volume may have contributed to averaging effects, which can obscure finer details in the penumbra region. The higher deviations in the penumbra region are partially caused by the secondary loss of electrons with small-volume detectors [9].

4.2. Isodose Lines

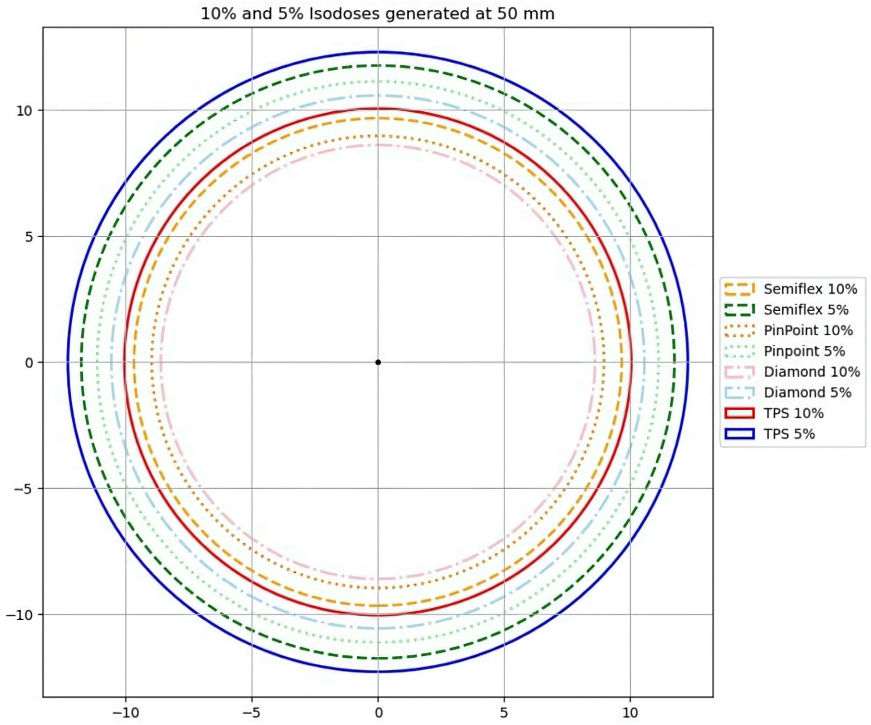

ISODOSE	TPS	SEMIFLEX 3D		PINPOINT 3D		MICRODIAMOND	
	X-POS (mm)	X-POS (mm)	DIFF. (mm)	X-POS (mm)	DIFF. (mm)	X-POS (mm)	DIFF. (mm)
10%	10.04	9.66	0.38	8.96	1.08	8.60	1.44
5%	12.28	11.75	0.53	11.12	1.16	10.56	1.72

Figure 3. Isodose lines differences at a penumbra region for three detectors and TPS generated profiles.

The decrement lines process, as explained in Section 2.3, was used to generate the isodose distributions of the raw and TPS generated data as shown on **Figure 3**. The isodose distributions were generated assuming circular symmetry. In practise, especially for larger field sizes, including diagonal beam-profile data in this analysis could serve as an extra means for comparison. The 10% and 5% isodose lines were analysed during this process, which were generated at a depth of 5 cm.

To analyse the isodose lines that were produced, the isodose lines generated using the TPS data were plotted against the lines generated using the experimental data collected using the three different detectors.

Semiflex 3D provides the closest measurements to TPS at both 10% and 5% isodose lines, suggesting it's more reliable in measuring the penumbra region. MicroDiamond despite being a high-resolution detector, shows the largest deviation. This could be due to over response in low- dose regions. Clinically, such differences can affect the perceived accuracy of dose delivery, especially in highly conformal techniques like stereotactic radiosurgery (SRS) or Intensity Modulated Radiotherapy. For penumbra analysis, Semiflex 3D appears to align better with the TPS. PinPoint 3D and microDiamond underestimate the dose fall off location, which could impact clinical evaluations if not accounted for. Understanding these discrepancies is crucial for detector selection in quality assurance and dosimetry verification.

5. Conclusions

This study underscores the critical importance of accurate penumbra characterization in small-field radiotherapy, particularly for high-precision treatments like stereotactic radiosurgery (SRS). Among the three detectors evaluated, the Semiflex 3D ion chamber consistently demonstrated the best agreement with TPS data across all field sizes, including the smallest 1×1 cm^2 field. Its larger collecting volume appears to contribute to more stable and accurate measurements in the penumbra region, even as field size decreases.

In contrast, the PinPoint 3D and microDiamond detectors—though designed for high-resolution measurements—exhibited larger deviations, particularly in very small fields, likely due to increased sensitivity to steep dose gradients and volume-averaging effects. Detector selection significantly influences penumbra measurement accuracy, especially in small fields. Semiflex 3D is the most reliable among the tested detectors for matching TPS predictions. Even with good correlation, systematic underestimation of penumbra width in small fields emphasizes the need for careful validation of detector performance.

The study contributes to clinical decision-making by informing users of detector selection during routine quality assurance (QA) and during treatment planning system (TPS) validation processes. For example, accurately characterizing the penumbra region is essential for commissioning beam data, especially for small-field IMRT, VMAT or stereotactic treatments. The findings suggest that the Semiflex 3D may offer a reliable balance between resolution and stability for routine QA, while the microDiamond could be prioritized for tasks requiring higher spatial accuracy in narrow fields.

Accurate dosimetry in small-field radiotherapy demands not only high-resolution detectors but also an understanding of their limitations. The Semiflex 3D stands out as the most appropriate choice in this study, reinforcing the need for appropriate detector selection to ensure precise dose delivery and safeguard sur-

rounding healthy tissue.

Conflicts of Interest

The authors declare no conflicts of interest regarding the publication of this paper.

References

[1] Malicki, J. (2012) The Importance of Accurate Treatment Planning, Delivery, and Dose Verification. *Reports of Practical Oncology & Radiotherapy*, **17**, 63-65. https://doi.org/10.1016/j.rpor.2012.02.001

[2] Cmrecak, F., Andrasek, I., Mekic, M.S., Ravlic, M. and Beketic-Oreskovic, L. (2019) Modern Radiotherapy Techniques. *Croatian Journal of Oncology*, **47**, 2-3.

[3] Friedman, W.A. and Bova, F.J. (1989) The University of Florida Radiosurgery System. *Surgical Neurology*, **32**, 334-342. https://doi.org/10.1016/0090-3019(89)90135-3

[4] Podgorsak, E.B., Bruce Pike, G., Pla, M., Olivier, A. and Souhami, L. (1990) Radiosurgery with Photon Beams: Physical Aspects and Adequacy of Linear Accelerators. *Radiotherapy and Oncology*, **17**, 349-358. https://doi.org/10.1016/0167-8140(90)90008-k

[5] Wilcox, E.E. and Daskalov, G.M. (2008) Accuracy of Dose Measurements and Calculations within and Beyond Heterogeneous Tissues for Photon Fields Smaller than Produced by Cyberknife. *Medical Physics*, **35**, 2259-2266. https://doi.org/10.1118/1.2912179

[6] Sharpe, M.B., Jaffray, D.A., Battista, J.J. and Munro, P. (1995) Extrafocal Radiation: A Unified Approach to the Prediction of Beam Penumbra and Output Factors for Megavoltage X-Ray Beams. *Medical Physics*, **22**, 2065-2074. https://doi.org/10.1118/1.597648

[7] Bova, F.J., Buatti, J.M., Friedman, W.A., Mendenhall, W.M., Yang, C. and Liu, C. (1997) The University of Florida Frameless High-Precision Stereotactic Radiotherapy System. *International Journal of Radiation Oncology, Biology, Physics*, **38**, 875-882. https://doi.org/10.1016/s0360-3016(97)00055-2

[8] Schulte, R.W., Fargo, R.A., Meinass, H.J., Slater, J.D. and Slater, J.M. (2000) Analysis of Head Motion Prior to and during Proton Beam Therapy. *International Journal of Radiation Oncology, Biology, Physics*, **47**, 1105-1110. https://doi.org/10.1016/s0360-3016(00)00551-4

[9] Hunt, M.A., Desobry, G.E., Fowble, B. and Coia, L.R. (1997) Effect of Low-Density Lateral Interfaces on Soft-Tissue Doses. *International Journal of Radiation Oncology, Biology, Physics*, **37**, 475-482. https://doi.org/10.1016/s0360-3016(96)00499-3

[10] Sharpe, M.B., Miller, B.M. and Wong, J.W. (2000) Compensation of X-Ray Beam Penumbra in Conformal Radiotherapy. *Medical Physics*, **27**, 1739-1745. https://doi.org/10.1118/1.1287283

[11] O'Malley, L., Pignol, J., Beachey, D.J., Keller, B.M., Presutti, J. and Sharpe, M. (2006) Improvement of Radiological Penumbra Using Intermediate Energy Photons (IEP) for Stereotactic Radiosurgery. *Physics in Medicine and Biology*, **51**, 2537-2548. https://doi.org/10.1088/0031-9155/51/10/012

[12] PTW (2017) Semiflex 3D Ion Chamber 31021. https://www.ptwdosimetry.com/en/products/semiflex-3d-ion-chamber-31021

[13] PTW (2018) PinPoint 3D Ion Chamber. https://www.ptwdosimetry.com/en/products/pinpoint-3d-ion-chamber

[14] PTW (2013) microDiamond. https://www.ptwdosimetry.com/en/products/microdiamond#c781

[15] Hidaytalla, L.A. (1994) Development of Isodose Curves for a 6MV X-Ray Beam. Master's Thesis, University of Khartoum.